Nano Research
2019, 12(6): 1467–1472

ISSN 1998-0124 CN 11-5974/O4
https://doi.org/10.1007/s12274-019-2413-9

Research Article

Synthesis of surface controlled nickel/palladium hydride nanodendrites with high performance in benzyl alcohol oxidation

Zipeng Zhao[1,§], Michelle M. Flores Espinosa[1,§], Jihan Zhou[2,4], Wang Xue[3], Xiangfeng Duan[3,4], Jianwei Miao[2,4], and Yu Huang[1,4] (✉)

[1] *Department of Materials Science and Engineering, University of California, Los Angeles, CA 90095, USA*
[2] *Department of Physics and Astronomy, University of California, Los Angeles, CA 90095, USA*
[3] *Department of Chemistry and Biochemistry, University of California, Los Angeles, CA 90095, USA*
[4] *California Nanosystems Institute, University of California, Los Angeles, CA 90095, USA*
[§] *Zipeng Zhao and Michelle M. Flores Espinosa contributed equally to this work.*

Received: 1 March 2019 / **Revised:** 8 April 2019 / **Accepted:** 9 April 2019

ABSTRACT

Benzaldehyde byproduct is an imperative intermediate in the production of fine chemicals and additives. Tuning selectivity to benzaldehyde is therefore critical in alcohol oxidation reactions at the industrial level. Herein, we report a simple but innovative method for the synthesis of palladium hydride and nickel palladium hydride nanodendrites with controllable morphology, high stability, and excellent catalytic activity. The synthesized dendrites can maintain the palladium hydride phase even after their use in the chosen catalytic reaction. Remarkably, the high surface area morphology and unique interaction between nickel-rich surface and palladium hydride (β-phase) of these nanodendrites are translated in an enhanced catalytic activity for benzyl alcohol oxidation reaction. Our Ni/$PdH_{0.43}$ nanodendrites demonstrated a high selectivity towards benzaldehyde of about 92.0% with a conversion rate of 95.4%, showing higher catalytic selectivity than their $PdH_{0.43}$ counterparts and commercial Pd/C. The present study opens the door for further exploration of metal/metal-hydride nanostructures as next-generation catalytic materials.

KEYWORDS

benzyl alcohol, selectivity, benzaldehyde, palladium hydride, oxidation, nanodendrites

1 Introduction

Noble metal nanostructures with controllable morphology possess multiple catalytic, electronic and optical properties which are indispensable for global industrial applications [1, 2]. Among them, dendritic nanostructures, have been widely attracted due to their highly branched and hierarchical structure ensuing large surface areas and unique catalytic, electronic and magnetic properties [3]. As a result of their high catalytic activity, nanodendritic structures with different compositions have been extensively studied in multiple oxidation-reduction reactions such as electrocatalytic oxidation of alcohols [4, 5] and oxidation of toxic compounds including benzene, toluene, and o-xylene in fuel [6]. Additionally, they have also been employed for oxygen-reduction reactions in fuel cells [7], reduction of 4-nitrophenol [8]. Beside those reactions, the selective oxidation reaction of primary alcohols to aldehydes is highly important for research at a laboratory and industrial scale as aldehydes are widely used in pharmaceutical industry and perfume business [9–11]. Specifically, tuning selectivity towards benzaldehyde is of great interest as it acts as an intermediate in the production of fine chemicals, and additives for flavoring and fragrance [12]. However, most of industrial alcohol oxidation reactions employ toxic chemicals as chromate, permanganate or peroxide components [13, 14]. Instead, other approaches like using pure oxygen as an oxidant in heterogeneous catalysis [15], provide a more green chemical process for the mentioned reaction. Enhancing the catalytic performance of noble metal nanocatalyst is critical for the environmentally friendly route of alcohol oxidation.

Palladium and palladium alloy catalysts have been found to be active for the oxidation of alcohols to their corresponding aldehydes and ketones [12, 15, 16]. Additionally, palladium hydrides present remarkable performance in hydrogen storage, sensing [17–19], and as a catalyst in multiple reactions. For instance, $PdH_{0.43}$ nanostructures have been employed as an anode for direct formic acid fuel cells, exhibiting higher mass activity at lower potentials than commercial Pd [20]. In the same way, $PdH_{0.43}$ nanocubes have shown enhanced selectivity of photocatalytic reduction of CO_2 into CH_4 [21]. Oxygen reduction reaction (ORR) has also been tested using palladium hydride nanocubes embedded in NiB nanosheets, showing an activity five times higher than Pt catalysts [22]. On the other hand, nickel has also been extensively used as a catalyst. For instance, interfaces created between Ni and CeO_2 on CNT have shown superior catalytic activity for hydrogen evolution reaction (HER) in alkaline solution, closest to the performance of Pt [23]. Gold-nickel bimetallic nanoparticles have also demonstrated enhanced activity for gas phase selective oxidation of alcohols [24]. Moreover, low cost and high hydrogen oxidation reaction (HOR) performance have been achieved with Ni@h-BN core–shell catalyst due to active h-BN/Ni interfaces formation [25]. Likewise, Pd-Ni nanostructures have been studied to achieve catalysts with lower cost and high performance for different chemical reactions. Recently bimetallic Pd-Ni icosahedra nanostructure with core rich in palladium and nickel decorating

Address correspondence to yhuang@seas.ucla.edu

the surface showed a dramatic improvement for ORR [26]. The Pd_6Ni icosahedra with Ni surface rich yielded higher ORR than those icosahedral structures with alloy surfaces or Pd-rich surfaces, proving that there is a unique and outstanding interaction between Pd core and Ni surface [26]. Other studies on Pd-Ni bimetallic structures have also considered high catalytic activity due to their interaction, for instance, in alcohol oxidation reactions as ethanol and formic acid oxidation [27, 28]. Hence, surface engineering techniques, like controlling surface facet [1, 15], or tuning surface composition [11, 29], can be a key for improving oxygen activation on palladium based nanoparticles which promotes selective oxidation of alcohol through a green chemistry route.

Here, we introduce an advanced yet straightforward set of steps to synthesize a new class of stable nanodendrites of palladium hydride ($PdH_{0.43}$) and nickel palladium hydride ($Ni/PdH_{0.43}$) with Ni tailored on the surface of $PdH_{0.43}$, exhibiting high selectivity towards the desired benzaldehyde in an advanced chemistry method. When compared to commercial Pd/C and $PdH_{0.43}$ compound, our synthesized $Ni/PdH_{0.43}$ dendrites show a dramatic improvement of their catalytic activity towards benzyl alcohol oxidation with high selectivity to benzaldehyde at high conversion rate demonstrating their potential use in new green routes for the synthesis of fine chemicals and organic intermediates [11].

2 Results and discussion

Palladium hydride ($PdH_{0.43}$) nanodendrites were first synthesized in one step method (for more details, see Experimental methods section). The material was then collected by centrifuge and washed several times with acetone/isopropanol mixture for further characterization (Fig. 1). Scanning transmission electron microscopy (STEM) image (Fig. 1(a)) and transmission electron microscopy (TEM) image of the as-synthesized $PdH_{0.43}$ material (Fig. 1(c) bottom left insert) confirm the formation of uniform dendrites. Additionally, selected area electron diffraction (SAED) pattern (Fig. 1(b)) of the selected dendrite $PdH_{0.43}$ (Fig. 1(b) top insert) shows clear concentric diffraction rings which can be indicated a face center cubic (fcc) crystalline structure. Further high resolution TEM (HRTEM) image (Fig. 1(c)) shows an average {111} interplane distance of 0.231 nm, again consistent with an fcc structure with a lattice parameter of around 0.400 nm. Powder X-ray diffraction (XRD) (Fig. 1(d)) pattern indicates an fcc structure with a lattice parameter of 0.3996 nm, consistent with SAED and HRTEM observations. HRTEM results and XRD pattern also indicate the formation of β-palladium hydride phase, corresponding to an H:Pd ratio of 0.43 as it was established in our earlier work [30], and in accordance with previous literatures [31–34].

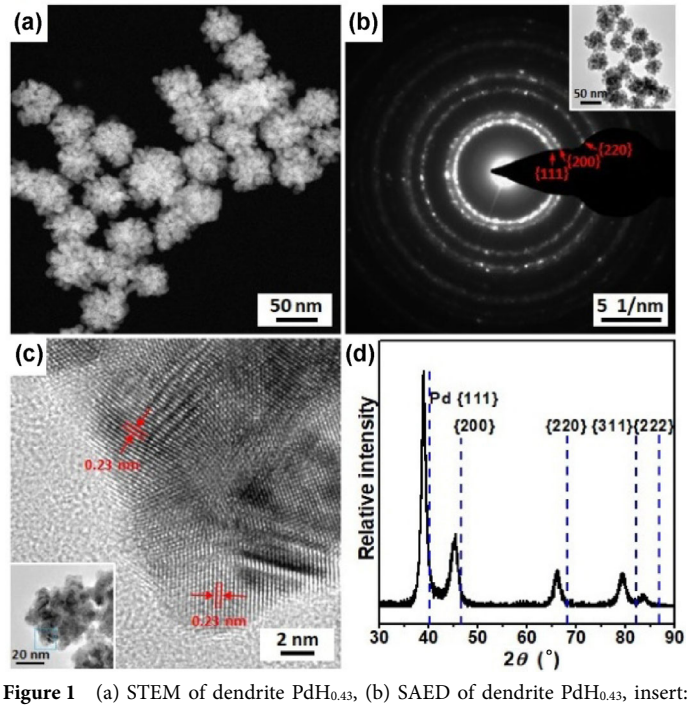

Figure 1 (a) STEM of dendrite $PdH_{0.43}$, (b) SAED of dendrite $PdH_{0.43}$, insert: TEM of dendrite $PdH_{0.43}$ showing the area for SAED, (c) HRTEM of dendrite $PdH_{0.43}$, insert: TEM image with blue rectangle indicates the area for HRTEM analysis, (d) powder XRD of dendrite $PdH_{0.43}$, blue perpendicular lines indicating the diffraction pattern position of Pd.

Meanwhile, time tracking studies (Fig. 2(a)) suggest that specific modification of different contents of hydrogen can be achieved by controlling the reaction time. In fact, after only 15 min of reaction, palladium hydride formation begins. XRD spectrum of the product collected at this time indicates a lattice parameter of 0.3942 nm, corresponding to an H:Pd ratio of about 0.22. At 30 min of the reaction, the XRD pattern confirms a higher H:Pd ratio around 0.30 with a lattice parameter of 0.3962 nm, which is consisted with the XRD peaks shift to a lower angle. As the synthesis time increases, the H:Pd ratio increases as well as it is showed after 1 h where XRD peaks are shifted to even a lower angle with a lattice parameter of 0.3990 nm, corresponding to a H:Pd ratio around 0.41. After 2 and 4 h, no significant shift of XRD peaks is observed, presenting a lattice parameter of 0.3996 nm and H:Pd ratio around 0.43 for both cases (Fig. 2(a) and Table S1 in the Electronic Supplementary Material (ESM)). The observed trend is consistent with our previous report [30]. In addition, the formation of $PdH_{0.43}$ phase is further confirmed by annealing test (Fig. 2(b)). After annealing the material for 2 h at a temperature of 400 °C in the argon atmosphere, palladium hydride nanodendrites transform back to its original state of pure palladium (Pd) due to desorption of hydrogen, showing a lattice parameter of 0.3890 nm corresponding to the observed shift of XRD peaks (Fig. 2(b)).

Moreover, the synthesized nanodendrites are found to be highly branched stable structures (Fig. 1(a)), and able to maintain composition and morphology when n-butylamine is introduced to the synthesis (for more details, see Experimental methods section). In fact, our studies demonstrate that the lack of this primary amine results in the absence of dendritic morphology (Fig. S1 in the ESM). TEM images (Figs. S1(a) and S1(c) in the ESM) of the synthesized materials without the primary amine showed a nanoflower-like shape instead without nanobranches. These observations are in agreement with previous studies that pointed out the importance of amine groups in their synthesis to develop stable nanostructures such as nanodendrites [5, 35]. In spite of their different morphology (with and without n-butylamine), the formation of β-palladium hydride phase is confirmed in both cases with SAED pattern (Fig. S1(b) in the ESM) which indicates an fcc packing structure with a lattice parameter around 0.400 nm which correspond to an H:Pd ratio of 0.43. HRTEM analysis of the same material (Fig. S1(c)

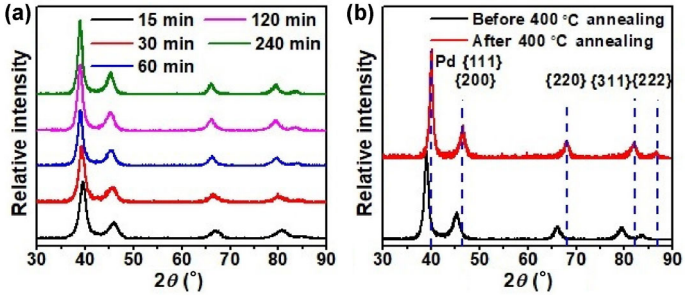

Figure 2 (a) Powder XRD tracking of dendrite $PdH_{0.43}$ synthesis at different time points, (b) annealing dendrite $PdH_{0.43}$ in Ar at 400 °C for 2 h showing powder XRD peaks shift from $PdH_{0.43}$ to palladium, blue perpendicular lines indicating the diffraction pattern position of Pd.

in the ESM) also proves the formation of hydride compound showing a {111} interplane *d*-spacing of around 0.231 nm indicating an fcc structure with a lattice parameter around 0.400 nm. Our observations suggest that the formation of hydride is originated from the catalytic decomposition of N,N-dimethylformamide (DMF), forming *in situ* $PdH_{0.43}$ compound whose transformation is independent of its morphology as established before [30].

In addition, we performed control experiments to replace our primary amine, n-butylamine, with ethylenediamine, triethylamine, or hydroxy-ethylamine while maintaining the other conditions the same. Our results show no formation of dendrites structure (Fig. S2 in the ESM) when using other types of amines but still formation of β-palladium hydride phase (Fig. S3 in the ESM) according to the XRD spectra, where XRD peaks are shifted to lower angles compared to those of pure Pd. These findings suggest that not all type of amines play a role for the successful development of dendritic morphologies. And the formation of palladium hydride phase is not impacted by the different type of amines since the hydrogen comes from the decomposition of DMF as it was discussed before [30]. Yet, n-butylamine proves indispensable for the formation of stable nanodendrites showing characteristics nanobranches (Fig. 1 and Fig. S2(a) in the ESM).

Subsequent to the success of $PdH_{0.43}$ dendrites synthesis, we move forward to a design of one-step synthesis to achieve $M/PdH_{0.43}$ dendritic nanostructure where M represents a metal, nickel (Ni) in this study. Bimetallic Pd-Ni nanoparticles with Ni-rich surface proved enhanced catalytic activity [26–28]. As a matter of fact, our $Ni/PdH_{0.43}$ dendrites show a much-improved catalytic selectivity and high activity towards benzyl alcohol oxidation reaction if compared with their counterpart $PdH_{0.43}$ dendrites and commercial Pd/C. $Ni/PdH_{0.43}$ dendrites were synthesized by mixing palladium(II) acetylacetonate ($Pd(acac)_2$), nickel(II) acetylacetonate ($Ni(acac)_2$), and n-butylamine in DMF (for more details, see Experimental methods section). The products were collected by centrifuge and washed several times with acetone/isopropanol mixture as in the same way of $PdH_{0.43}$ dendrites. Further characterization was performed on the collected material (Fig. 3). TEM image (Fig. 3(a)) confirms the development of the uniform nanodendritic structures. Powder XRD (Fig. 3(b)) pattern indicates an fcc packing structure with a lattice parameter of 0.3996 nm indicating the presence of β-palladium hydride phase with an H:Pd ratio of around 0.43, same as the case of $PdH_{0.43}$ dendrites. The Ni:Pd ratio is found to be 0.17 based on the energy dispersive spectroscopy (EDS). Similarly, HRTEM analysis (Fig. 3(c)) indicates an average {111} interplane distance of about 0.231 nm matching a lattice parameter of about 0.400 nm, confirming the presence of β-palladium hydride phase. It should be highlighted that, in powder XRD and HRTEM results, palladium hydride is the dominant phase. In this context, Ni content in the product seems not to form an alloy compound with palladium. Therefore, these findings suggest an initial development of $PdH_{0.43}$ seeds, followed by the reduction of Ni and growth onto $PdH_{0.43}$ surface, ending with a $Ni/PdH_{0.43}$ structure. In fact, EDS map image shows clearly a high concentration of palladium at the core whereas nickel is mostly enriched on the surface (Fig. 3(d) and Fig. S4 in the ESM). Green arrows in HRTEM images (Fig. 3(c)) indicate the formation of islands with different contrast from the internal structure suggesting a nickel content on the outmost surface on palladium hydride in accordance with previous evidence. To asses surface properties and oxidation states of the metals on both dendrites, which are $PdH_{0.43}$, and $Ni/PdH_{0.43}$, X-ray photoelectron spectroscopy (XPS) was employed (Fig. 4). The Pd 3d spectra of both dendrites (Figs. 4(a) and 4(c), respectively) confirm the Pd is mainly in Pd^0 metallic state. In the case of Ni in $Ni/PdH_{0.43}$ nanodendrites, the Ni is found to be around 40.3% of metallic Ni^0, and a 59.7% of Ni^{2+} (Fig. 4(e)).

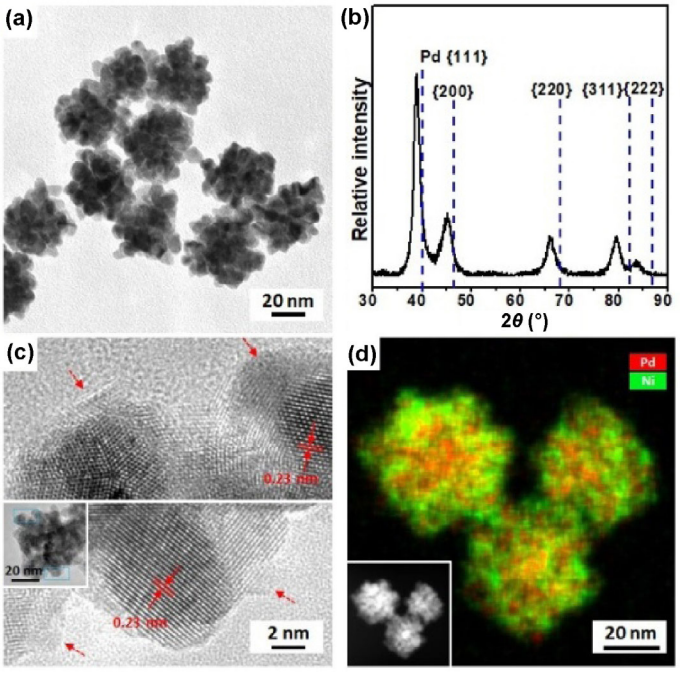

Figure 3 (a) TEM image of dendriet $Ni/PdH_{0.43}$. (b) Powder XRD of dendriet $Ni/PdH_{0.43}$, blue perpendicular lines indicating the diffraction pattern position of Pd. (c) HRTEM image of $Ni/PdH_{0.43}$, bottom insert: zoom out image showing the area for HRTEM with blue rectangle. (d) EDS map of Pd (red) and Ni (green) distribution, bottom insert: STEM image of same area.

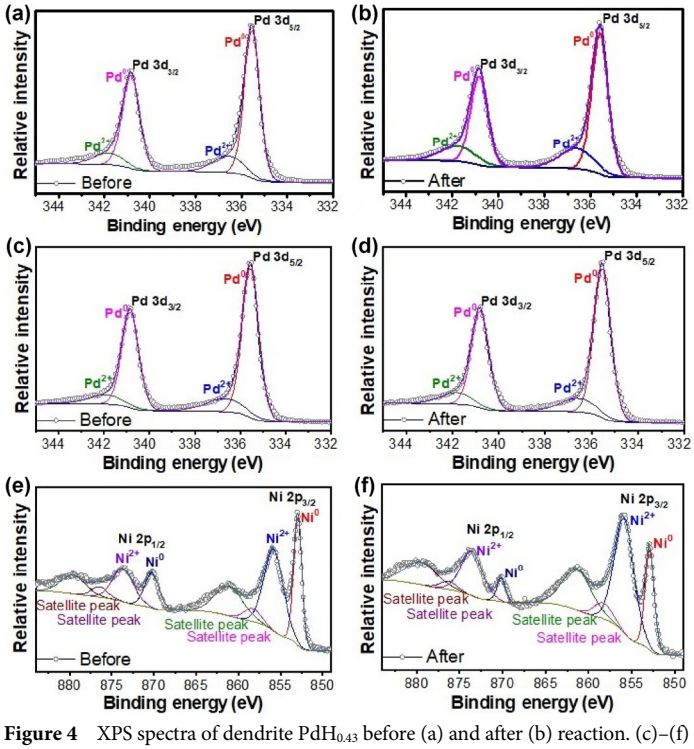

Figure 4 XPS spectra of dendrite $PdH_{0.43}$ before (a) and after (b) reaction. (c)–(f) XPS spectra of dendrite $Ni/PdH_{0.43}$ before (c) and (e) and after (d) and (f) reaction.

Similar to $PdH_{0.43}$ nanodendrite studies, control experiment without n-butylamine is also performed for $Ni/PdH_{0.43}$ synthesis (Fig. S5 in the ESM), confirming once again no formation of dendrites in the absence of the primary amine (Fig. S5(a) in the ESM) but still formation of β-palladium hydride phase as it is observed from the XRD pattern (Fig. S5(b) in the ESM). The above results also suggest that $PdH_{0.43}$ formation happens first, soon after the temperature of decomposition of DMF is reached, following by the surface coverage of nickel.

Finally, to assess the catalytic activity of our synthesized dendrites nanomaterials, selective oxidation of benzyl alcohol reaction was used as the model reaction. The reaction was performed by dispersing 5 mg of Pd for as catalyst on 2 mL of benzyl alcohol. The reaction was kept at 100 °C in 2 atm of oxygen. We found that for the products of the benzyl alcohol oxidation reaction, that is, toluene, benzaldehyde, benzoic acid, and benzyl benzoate (Table 1), $Ni/PdH_{0.43}$ dendrites exhibit the highest selectivity towards benzaldehyde with a value of 92% and still at a high conversion rate of 95.4% if compared with the selectivity of 71.8% and 53.5%, and conversion rate of 97% and 96.4% of $PdH_{0.43}$ dendrites and commercial Pd/C respectively (see the ESM for details). Considering that $Ni/PdH_{0.43}$ and $PdH_{0.43}$ nanodendrites are similar in morphology, size and hydride composition, it is reasonable to suggest that the excellent selectivity to benzaldehyde of $Ni/PdH_{0.43}$ is attributed to the nickel-rich surface onto the $PdH_{0.43}$ core of $Ni/PdH_{0.43}$ compound.

After testing the model reaction, our catalysts were collected for further stability characterization (Fig. S7 in the ESM). The outstanding stability of our dendrites is also confirmed by XRD spectra where palladium hydride and nickel/palladium hydride dendrites maintained the hydride phase, presenting a lattice parameter of about 0.3996 nm which correspond to the H:Pd ratio of 0.43 (Fig. S7 in the ESM).

Additionally, XPS spectra of $PdH_{0.43}$ and $Ni/PdH_{0.43}$ dendrites before and after reaction (Fig. 4) reveal no significant difference in their Pd and Ni chemical states. For instance, XPS spectrum of the initial $PdH_{0.43}$ dendrites exposes a Pd^0 metallic state of around 81.1% (Fig. 4(a)) versus a Pd^0 76.9% after the catalytic reaction (Fig. 4(b)). In a similar way, the initial $Ni/PdH_{0.43}$ dendrites showed an initial metallic state of 83.4% Pd^0 and 40.3% Ni^0 (Figs. 4(c) and 4(e), respectively) versus an 83.8% Pd^0 and 29.2% Ni^0 after reaction (Figs. 4(d) and 4(f), respectively). Thus, chemical states of the tested catalysts are not significantly changed even after the benzyl alcohol oxidation reaction.

To further confirm high selectivity towards benzaldehyde due to the unique interaction between the Ni-rich surface and $PdH_{0.43}$, we tested the benzyl alcohol oxidation reaction on $Ni/PdH_{0.43}$ and Pd-Ni alloy again with carbon black support. In a typical procedure, $Ni/PdH_{0.43}$/C was synthesized first, washed and collected (for more details, see Experimental methods section). Pd-Ni/C material was obtained by annealing $Ni/PdH_{0.43}$/C powder at 400 °C in an argon atmosphere for 2 h (Fig. S8(a) in the ESM). Further characterization was performed on both nanostructures (Fig. S8 in the ESM). TEM images of $Ni/PdH_{0.43}$/C and Pd-Ni/C catalysts (Figs. S8(b) and S8(c) in the ESM) proved that both materials maintain similar size and morphology, therefore, serve as a comparison between hydride $Ni/PdH_{0.43}$ and non-hydride Pd-Ni(alloy) materials. XRD spectrum (Fig. S8(d) in the ESM) also proves the complete transformation of $Ni/PdH_{0.43}$/C (black line) to Pd-Ni/C (red line) where the peaks are shifted to higher angles, showing the formation of Pd-Ni alloy on carbon support.

Table 1 Performance comparison for Pd/C, dendrite $PdH_{0.43}$, and dendrite $Ni/PdH_{0.43}$. Benzyl alcohol oxidation conversion and product selectivity. The turnover frequency (TOF) calculation is based on 3 h of measurements

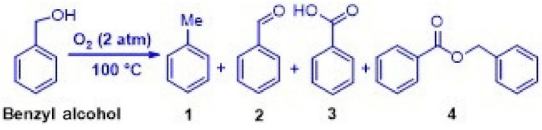

Catalyst	Conversion (%)	Selectivity (%)				TOF (s^{-1})
		1	2	3	4	
Pd	96.4	37.4	53.5	1.3	7.8	0.11
$PdH_{0.43}$	97.0	28.1	71.8	0	0	0.76
$Ni/PdH_{0.43}$	95.4	7.2	92.0	0	0.8	0.74

Lastly, benzyl alcohol oxidation reaction of the developed catalysts (Table S2 in the ESM) confirmed higher catalytic activity for the hydride compound ($Ni/PdH_{0.43}$/C) than non-hydride compound (Pd-Ni/C). This is also attributed to the fact that Pd-Ni/C is forming an alloy rather than a Ni surface rich on $PdH_{0.43}$, once again proving the unique feature of our synthesized $Ni/PdH_{0.43}$ nanodendrites. For instance, $Ni/PdH_{0.43}$/C material exhibited a superior selectivity towards benzaldehyde of 90.2% and a conversion rate of 95.1%, whereas the non-hydride alloy Pd-Ni/C showed a lower selectivity of 82.9% and conversion rate of 94.3%. These results suggest that Ni modified the $PdH_{0.43}$ surface presents advantages over Pd-Ni alloy, which agrees with our previous observations (Fig. 3 and Fig. S4 in the ESM, Table 1).

3 Conclusion

In summary, we have successfully developed $PdH_{0.43}$ and $Ni/PdH_{0.43}$, a new class of stable nanodendritic hydride materials. $PdH_{0.43}$ and $Ni/PdH_{0.43}$ are found to be good nanostructures showing remarkable stability in what refers to composition and phase. In terms of catalytic activity, both nanostructures exhibited outstanding catalytic activity, higher than commercial Pd/C due to its composition and dendritic structure. In fact, our synthesized $Ni/PdH_{0.43}$ nanodendrites showed the highest selectivity and conversion rate of all of them. The experimental evidence revealed that the enhancement of selectivity to benzaldehyde of $Ni/PdH_{0.43}$ was mainly attributed to the synergistic of the Ni-rich surface and the $PdH_{0.43}$. The newly developed $Ni/PdH_{0.43}$ nanodendrites demonstrate their potential in applications towards greener process in benzyl alcohol oxidation reactions through the combined morphology and controlled surface composition to tune selectivity towards benzaldehyde.

4 Experimental methods

4.1 Chemicals and materials

$Pd(acac)_2$, $Ni(acac)_2$, sodium tetrachloropalladate(II) (Na_2PdCl_4), n-butylamine, ethylenediamine, trimethylamine, hydroxyethylamine, Pd/C (10% Pd) were purchased from Sigma Aldrich. DMF, acetone and isopropanol were purchased from Fisher Scientific. Ethanol was purchased from Decon Labs, Inc. Vulcan XC-72 carbon black was obtained from Cabot Corporation. Water used was Ultrapure Millipore (18.2 MΩ·cm).

4.2 Synthesis of $PdH_{0.43}$ nanodendrites

8 mg of $Pd(acac)_2$, 100 μL of n-butylamine was dissolved in 10 mL of DMF within 25 mL vial was heated at 160 °C in an oil bath for 4 h. The obtained nanomaterials were separated from solvent through centrifugation and then washed with acetone/isopropanol three times. Time tracking studies during synthesis of hydride dendrites were performed from 15 to 240 min.

4.3 Control experiments for replacing small molecules

8 mg $Pd(acac)_2$ and 100 μL of small molecules (ethylenediamine, triethylamine or hydroxyethylamine) were dissolved in 10 mL DMF within a 25 mL glass vial. The sealed vial was kept at 160 °C for 4 h. The obtained nanomaterials were separated from solvent through centrifugation and then washed with acetone/isopropanol three times.

4.4 Synthesis of $Ni/PdH_{0.43}$ nanodendrites

10 mg of $Pd(acac)_2$, 5 mg $Ni(acac)_2$, 50 μL of n-butylamine was dissolved in 10 mL of DMF within 25 mL vial was heated at 160 °C in an oil bath for 12 h. The obtained nanomaterials were separated from solvent through centrifugation and then washed with acetone/isopropanol three times.

4.5 Synthesis of nanoparticle Ni/$PdH_{0.43}$/C

14 mg carbon black was dissolved in 9 mL of DMF. Then, 8 mg of $Pd(acac)_2$, 4 mg $Ni(acac)_2$, was dissolved in 1 mL of DMF and mixed with 9 mL DMF solution, which contained carbon black, within a 25 mL vial. The vial was heated at 160 °C in an oil bath for 12 h. The obtained nanomaterials were separated from solvent through centrifugation and then washed with acetone/isopropanol three times.

4.6 Synthesis of nanoparticle Pd-Ni/C

The obtained nanoparticle Ni/$PdH_{0.43}$/C powder was annealed in Ar atmosphere for 2 h at 400 °C. Through the annealing, the Ni/$PdH_{0.43}$/C was converted to nanoparticle Pd-Ni/C.

4.7 Characterization

TEM images were taken on an FEI T12 transmission electron microscope operated at 120 kV. HRTEM images and SAED were taken on an FEI Titan transmission electron microscope operated at 300 kV. EDS mapping and high angle annular dark field (HAADF)-STEM image were taken on a Titan X operated at 200 kV. The samples were prepared by dropping ethanol dispersion of samples onto carbon-coated copper TEM grids (Ladd Research, Williston, VT, USA) using pipettes and dried under ambient condition. Powder XRD patterns were collected on a Panalytical X'Pert Pro X-ray Powder Diffractometer with Cu-Kα radiation. XPS tests were done with Kratos AXIS Ultra DLD spectrometer.

4.8 Catalysis study

For benzyl alcohol catalytic oxidation study, the Pd loading in each catalysis study was maintained to be 5 mg (commercial Pd/C, dendrite $PdH_{0.43}$, or dendrite Ni/$PdH_{0.43}$ used as a catalyst) and the amount of benzyl alcohol was maintained to be 2 mL for each catalytic test. The catalyst is dispersed in 2 mL benzyl alcohol, and no additional solvent is needed. The catalysis was carried out at 100 °C in oxygen with a pressure of 2 atm.

When particle Ni/$PdH_{0.43}$/C or particle Pd-Ni/C used as a catalyst, the Pd loading in each catalysis study was maintained to be 10 mg for each catalysis study. After catalysis, the catalyst was separated from the product by centrifugation. Then the product was diluted with acetone for further composition analysis. Chemical composition analysis was done by gas chromatography-mass spectroscopy (GC-MS; Shimadzu GCMS-QP2010 Plus).

Turnover frequency (TOF) is reported based on the turnover number per unit time (TOF = TON/time), where TON = (number of reactant converted)/(total active sites of catalyst).

Acknowledgements

Y. H., X. D., Z. Z., and M. F. E. acknowledge the support from Office of Naval Research by the grant number of N000141812155. J. Z. and J. M. acknowledge the support from Office of Basic Energy Sciences of the US DOE (No. DE-SC0010378). The HAADF-STEM imaging and EDS mapping with Titan X were performed at the Molecular Foundry, which is supported by the Office of Science, Office of Basic Energy Sciences of the U.S. DOE under Contract No. DE-AC02—05CH11231.

Electronic Supplementary Material: Supplementary material (characterization results and additional catalysis reaction results) is available in the online version of this article at https://doi.org/10.1007/s12274-019-2413-9.

References

[1] Tian, N.; Zhou, Z. Y.; Sun, S. G.; Ding, Y.; Wang, Z. L. Synthesis of tetrahexahedral platinum nanocrystals with high-index facets and high electro-oxidation activity. *Science* **2007**, *316*, 732–735.

[2] Wu, Z. C.; Zhang, Y.; Wang, B.; Qian, G. X.; Tao, T. X. Synthesis of palladium dendritic nanostructures on amidoxime modified polyacrylonitrile fibers through a complexing-reducing method. *Mater. Sci. Eng. B* **2013**, *178*, 923–929.

[3] Zhu, G. M.; Jiang, Y. Y.; Lin, F.; Zhang, H.; Jin, C. H.; Yuan, J.; Yang, D. R.; Zhang, Z. *In situ* study of the growth of two-dimensional palladium dendritic nanostructures using liquid-cell electron microscopy. *Chem. Commun*. **2014**, *50*, 9447–9450.

[4] Eid, K.; Ahmad, Y. H.; Yu, H. J.; Li, Y. H.; Li, X. N.; AlQaradawi, S. Y.; Wang, H. L.; Wang, L. Rational one-step synthesis of porous PtPdRu nanodendrites for ethanol oxidation reaction with a superior tolerance for CO-poisoning. *Nanoscale* **2017**, *9*, 18881–18889.

[5] Lu, L. F.; Chen, S. T.; Thota, S.; Wang, X. D.; Wang, Y. C.; Zou, S. H.; Fan, J.; Zhao, J. Composition controllable synthesis of PtCu nanodendrites with efficient electrocatalytic activity for methanol oxidation induced by high index surface and electronic interaction. *J. Phys. Chem. C* **2017**, *121*, 19796–19806.

[6] da Silva, A. G. M.; Rodrigues, T. S.; Slater, T. J. A.; Lewis, E. A.; Alves, R. S.; Fajardo, H. V.; Balzer, R.; da Silva, A. H. M.; de Freitas, I. C.; Oliveira, D. C. et al. Controlling size, morphology, and surface composition of AgAu nanodendrites in 15 s for improved environmental catalysis under low metal loadings. *ACS Appl. Mater. Interfaces* **2015**, *7*, 25624–25632.

[7] Fu, S. F.; Zhu, C. Z.; Shi, Q. R.; Xia, H. B.; Du, D.; Lin, Y. H. Highly branched PtCu bimetallic alloy nanodendrites with superior electrocatalytic activities for oxygen reduction reactions. *Nanoscale* **2016**, *8*, 5076–5081.

[8] Zhang, X. F.; Zhu, X. Y.; Feng, J. J.; Wang, A. J. Solvothermal synthesis of N-doped graphene supported PtCo nanodendrites with highly catalytic activity for 4-nitrophenol reduction. *Appl. Surf. Sci*. **2018**, *428*, 798–808.

[9] Pillai, U. R.; Sahle-Demessie, E. Sn-exchanged hydrotalcites as catalysts for clean and selective Baeyer–Villiger oxidation of ketones using hydrogen peroxide. *J. Mol. Catal. A*: *Chem*. **2003**, *191*, 93–100.

[10] Meng, C.; Yang, K.; Fu, X. Z.; Yuan, R. S. Photocatalytic oxidation of benzyl alcohol by homogeneous $CuCl_2$/solvent: A model system to explore the role of molecular oxygen. *ACS Catal*. **2015**, *5*, 3760–3766.

[11] Enache, D. I.; Edwards, J. K.; Landon, P.; Solsona-Espriu, B.; Carley, A. F.; Herzing, A. A.; Watanabe, M.; Kiely, C. J.; Knight, D. W.; Hutchings, G. J. Solvent-free oxidation of primary alcohols to aldehydes using Au-Pd/TiO_2 catalysts. *Science* **2006**, *311*, 362–365.

[12] Galvanin, F.; Sankar, M.; Cattaneo, S.; Bethell, D.; Dua, V.; Hutchings, G. J.; Gavriilidis, A. On the development of kinetic models for solvent-free benzyl alcohol oxidation over a gold-palladium catalyst. *Chem. Eng. J*. **2018**, *342*, 196–210.

[13] Pillai, U. R.; Sahle-Demessie, E. Oxidation of alcohols over Fe^{3+}/montmorillonite-K10 using hydrogen peroxide. *Appl. Catal. A*: *Gen*. **2003**, *245*, 103–109.

[14] Sheldon, R. A.; Kochi, J. K. *Metal-Catalyzed Oxidations of Organic Compounds*: *Mechanistic Principles and Synthetic Methodology Including Biochemical Processes*; Academic Press: New York, 1981.

[15] Long, R.; Mao, K. K.; Ye, X. D.; Yan, W. S.; Huang, Y. B.; Wang, J. Y.; Fu, Y.; Wang, X. S.; Wu, X. J.; Xie, Y. et al. Surface facet of palladium nanocrystals: A key parameter to the activation of molecular oxygen for organic catalysis and cancer treatment. *J. Am. Chem. Soc*. **2013**, *135*, 3200–3207.

[16] Mori, K.; Hara, T.; Mizugaki, T.; Ebitani, K.; Kaneda, K. Hydroxyapatite-supported palladium nanoclusters: A highly active heterogeneous catalyst for selective oxidation of alcohols by use of molecular oxygen. *J. Am. Chem. Soc*. **2004**, *126*, 10657–10666.

[17] Liang, H. P.; Lawrence, N. S.; Wan, L. J.; Jiang, L.; Song, W. G.; Jones, T. G. J. Controllable synthesis of hollow hierarchical palladium nanostructures with enhanced activity for proton/hydrogen sensing. *J. Phys. Chem. C* **2008**, *112*, 338–344.

[18] Yamauchi, M.; Ikeda, R.; Kitagawa, H.; Takata, M. Nanosize effects on hydrogen storage in palladium. *J. Phys. Chem. C* **2008**, *112*, 3294–3299.

[19] Kumara, L. S. R.; Sakata, O.; Kobayashi, H.; Song, C.; Kohara, S.; Ina, T.; Yoshimoto, T.; Yoshioka, S.; Matsumura, S.; Kitagawa, H. Hydrogen storage and stability properties of Pd–Pt solid-solution nanoparticles revealed via atomic and electronic structure. *Sci. Rep*. **2017**, *7*, 14606.

[20] Zhang, J. W.; Chen, M. S.; Li, H. Q.; Li, Y. J.; Ye, J. Y.; Cao, Z. M.; Fang, M. L.; Kuang, Q.; Zheng, J.; Xie, Z. X. Stable palladium hydride as a superior

anode electrocatalyst for direct formic acid fuel cells. *Nano Energy* **2018**, *44*, 127–134.

[21] Zhu, Y. Z.; Gao, C.; Bai, S.; Chen, S. M.; Long, R.; Song, L.; Li, Z. Q.; Xiong, Y. J. Hydriding Pd cocatalysts: An approach to giant enhancement on photocatalytic CO_2 reduction into CH_4. *Nano Res*. **2017**, *10*, 3396–3406.

[22] Lu, Y. Z.; Wang, J.; Peng, Y. C.; Fisher, A.; Wang, X. Highly efficient and durable Pd hydride nanocubes embedded in 2D amorphous NiB nanosheets for oxygen reduction reaction. *Adv*. *Energy Mater*. **2017**, *7*, 1700919.

[23] Weng, Z.; Liu, W.; Yin, L. C.; Fang, R. P.; Li, M.; Altman, E. I.; Fan, Q.; Li, F.; Cheng, H. M.; Wang, H. L. Metal/oxide interface nanostructures generated by surface segregation for electrocatalysis. *Nano Lett*. **2015**, *15*, 7704–7710.

[24] Yi, W. Z.; Yuan, W. T.; Meng, Y.; Zou, S. H.; Zhou, Y. H.; Hong, W.; Che, J. W.; Hao, M. J.; Ye, B.; Xiao, L. P. et al. A rational solid-state synthesis of supported Au–Ni bimetallic nanoparticles with enhanced activity for gas-phase selective oxidation of alcohols. *ACS Appl*. *Mater*. *Interfaces* **2017**, *9*, 31853–31860.

[25] Gao, L. J.; Wang, Y.; Li, H. B.; Li, Q. H.; Ta, N.; Zhuang, L.; Fu, Q.; Bao, X. H. A nickel nanocatalyst within a h-BN shell for enhanced hydrogen oxidation reactions. *Chem*. *Sci*. **2017**, *8*, 5728–5734.

[26] Feng, Y. G.; Shao, Q.; Ji, Y. J.; Cui, X. N.; Li, Y. Y.; Zhu, X.; Huang, X. Q. Surface-modulated palladium-nickel icosahedra as high-performance non-platinum oxygen reduction electrocatalysts. *Sci*. *Adv*. **2018**, *4*, eaap8817.

[27] Obradović, M. D.; Stančić, Z. M.; Lačnjevac, U. Č.; Radmilović, V. V.; Gavrilović-Wohlmuther, A.; Radmilović, V. R.; Gojković, S. L. Electrochemical oxidation of ethanol on palladium-nickel nanocatalyst in alkaline media. *Appl*. *Catal*. *B*: *Environ*. **2016**, *189*, 110–118.

[28] Jiang, S. F.; Yi, B. L.; Zhao, Q.; Yu, H. M.; Shao, Z. G. Palladium–nickel catalysts based on ordered titanium dioxide nanorod arrays with high catalytic peformance for formic acid electro-oxidation. *RSC Adv*. **2017**, *7*, 11719–11723.

[29] Dimitratos, N.; Lopez-Sanchez, J. A.; Morgan, D.; Carley, A. F.; Tiruvalam, R.; Kiely, C. J.; Bethell, D.; Hutchings, G. J. Solvent-free oxidation of benzyl alcohol using Au-Pd catalysts prepared by sol immobilisation. *Phys*. *Chem*. *Chem*. *Phys*. **2009**, *11*, 5142–5153.

[30] Zhao, Z. P.; Huang, X. Q.; Li, M. F.; Wang, G. M.; Lee, C.; Zhu, E. B.; Duan, X. F.; Huang, Y. Synthesis of stable shape-controlled catalytically active β-palladium hydride. *J*. *Am*. *Chem*. *Soc*. **2015**, *137*, 15672–15675.

[31] Wolf, R. J.; Lee, M. W.; Davis, R. C.; Fay, P. J.; Ray, J. R. Pressure-composition isotherms for palladium hydride. *Phys*. *Rev*. *B* **1993**, *48*, 12415–12418.

[32] Flanagan, T. B.; Oates, W. A. The palladium-hydrogen system. *Annu*. *Rev*. *Mater*. *Sci*. **1991**, *21*, 269–304.

[33] Eastman, J. A.; Thompson, L. J.; Kestel, B. J. Narrowing of the palladium-hydrogen miscibility gap in nanocrystalline palladium. *Phys*. *Rev*. *B* **1993**, *48*, 84–92.

[34] Schirber, J. E.; Morosin, B. Lattice constants of β-PdH*x* and β-PdD*x* with *x* near 1.0. *Phys*. *Rev*. *B* **1975**, *12*, 117–118.

[35] Xue, Z. H.; Li, M. Q.; Rao, H. H.; Yin, B.; Zhou, X. B.; Liu, X. H.; Lu, X. Q. Phase transformation-controlled synthesis of CuO nanostructures and their application as an improved material in a carbon-based modified electrode. *RSC Adv*. **2016**, *6*, 12829–12836.